

Operando XAS/SAXS: Guiding Design of Single-Atom and Subnanocluster Catalysts

Lingzhe Fang, Soenke Seifert, Randall E. Winans, and Tao Li*

Single-atom and subnanocluster catalysts (SSCs) represent a highly promising class of low-cost materials with high catalytic activity and high atom-utilization efficiency. However, SSCs are susceptible to undergo restructuring during the reactions. Exploring the active sites of catalysts through in situ characterization techniques plays a critical role in studying reaction mechanism and guiding the design of optimum catalysts. In situ X-ray absorption spectroscopy/small-angle X-ray scattering (XAS/SAXS) is promising and widely used for monitoring electronic structure, atomic configuration, and size changes of SSCs during real-time working conditions. Unfortunately, there is no detailed summary of XAS/SAXS characterization results of SSCs. The recent advances in applying in situ XAS/SAXS to SSCs are thoroughly summarized in this review, including the atomic structure and oxidation state variations under open circuit and realistic reaction conditions. Furthermore, the reversible transformation of single-atom catalysts (SACs) to subnanoclusters/nanoparticles and the application of in situ XAS/SAXS in subnanoclusters are discussed. Finally, the outlooks in modulating the SSCs and developing operando XAS/SAXS for SSCs are highlighted.

site consisting of the single metal atom and coordinated atoms in SACs, thereby improving the selectivity of products for catalytic reactions. Moreover, atomically dispersed metal catalysts exist in cations, which exhibit better stability than traditional nanosized counterparts.^[10] Subnanocluster catalysts, which are between SACs and nanocatalysts, preserve sufficient reaction active sites and, at the same time, lowered oxidation state of constituent atoms. In the energy conversion area, the metallic/low valence state of catalysts are beneficial for some catalytic reduction reactions.^[11]

However, SSCs face characterization difficulties, especially under working conditions. X-ray diffraction is unable to detect atomic-scale catalysts formed by the aggregation of only a few atoms, not to mention SACs. Even though aberration-corrected transmission electron microscopy (TEM) with atomic resolution


can observe geometric configurations of SSCs. It is still difficult to monitor the changes of catalysts during the reaction conditions directly in most cases. Besides, in situ Fourier-transform infrared spectroscopy (FTIR) has been employed to distinguish between single atoms (SAs) and dimer/clusters/nanoparticles by study the vibration mode of the adsorbed CO molecule on catalyst.^[12,13] But exploring the evolution of the electronic and atomic structure of SACs by in situ FTIR under real-time working conditions is still underdeveloped. Additionally, when the SACs loading is very low, the catalysts' oxidation state, which is highly correlated with the catalytic activity, cannot be accurately detected by X-ray photoelectron spectroscopy (XPS). In contrast, as a synchrotron-based element-specific technique, X-ray absorption spectroscopy (XAS) is influential in studying the probed element's structural information.^[14–17] By exciting an electron from the core to an unoccupied band, the obtained XAS spectrum can be divided into X-ray absorption near edge structure (XANES) and extended X-ray absorption fine structure (EXAFS) (Figure 1a). XANES spectra reflect electronic structure while EXAFS spectra provide local atomic structural information, such as coordination number, bond length, and structural disorder. Besides, sometimes the aggregation of SSCs into larger sized catalysts will occur during the synthesis or reaction process. Compared with X-ray diffraction that is applied to study lattice information of crystal matter, small-angle X-ray scattering (SAXS) is used to collect the variation of X-ray scattering intensity with a small q value.^[18,19] According

1. Introduction

With the development of synthesis technologies and characterization methods, single-atom and subnanocluster catalysts (SSCs) have attracted much attention. Due to the size-dependent catalytic performance, SSCs exhibit higher catalytic activities than the corresponding nanosized catalysts.^[1–3] Benefit from the maximum atom-utilization efficiency and tunable coordination environment, the uniformly dispersed single-atom catalysts (SACs) on diverse supports have been widely applied in the field of energy conversion and storage.^[4–9] More importantly, different from the multiple crystal facets of nanomaterials can serve as active sites, there is only one active

L. Fang, Prof. T. Li
Department of Chemistry and Biochemistry
Northern Illinois University
DeKalb, IL 60115, USA
E-mail: tli4@niu.edu

Dr. S. Seifert, Dr. R. E. Winans, Prof. T. Li
Chemistry and Material Science Group
X-ray Science Division
Argonne National Laboratory
Lemont, IL 60439, USA

 The ORCID identification number(s) for the author(s) of this article can be found under <https://doi.org/10.1002/smt.202001194>.

DOI: 10.1002/smt.202001194

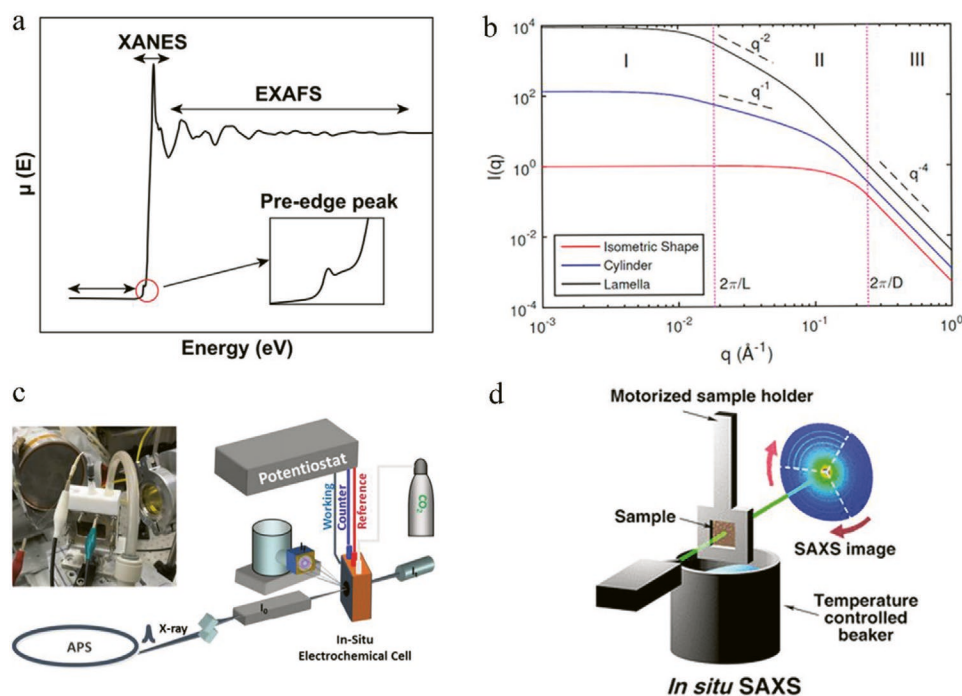


Figure 1. a) Schematic of XAS spectra. Reproduced with permission.^[33] Copyright 2019, Springer Nature. b) Calculated form factor scatterings of objects with various dimensions and sharp interfaces. Reproduced with permission.^[19] Copyright 2016, American Chemical Society. c) Schematics of in situ XAS experimental set-up at the advanced photon source. Reproduced with permission.^[22] Copyright 2020, Springer Nature. d) Schematics of setup for the in situ SAXS. Reproduced with permission.^[95] Copyright 2018, American Chemical Society.

to the Bragg's law, SAXS is useful to study large distance structures information (including size and shape) of the matter at the nanoscale (Figure 1b). Unlike the analysis area limitation of TEM, SAXS provides structural information averaged over a macroscopic range. Even though SAXS is widely used in nanoparticle research,^[19,20] it is able to probe clusters of dozens or even several atoms.

Mostly, the physicochemical properties of catalysts will not remain unchanged during the reaction. SACs would self-adjust to promote the catalytic reaction.^[11] Thus, the identification of active sites is essential for studying the catalytic mechanism. However, oxygen in the air, electrolyte environment under open-circuit voltage (OCV), and applied potential conditions significantly impact the environmentally sensitive SSCs. This leads to the ex situ characterizations of post-reaction SSCs are almost meaningless. For example, the observation results of SACs by in situ and ex situ XAS are usually different.^[21–25] Agglomerated SACs can be oxidized into the initial high-valence SACs at post-catalysis conditions.^[22,23] Compared to ex situ XAS, in situ XAS unfolds incomparable merits of identifying catalytic sites via capturing oxidation state and local geometric configuration variations under real-time working conditions, which provides clues on how SSCs work at the atomic level (Figure 1c). With the aid of density functional theory (DFT) calculations, the hypothesized reaction mechanism can be put forward. Moreover, in situ SAXS provides an ideal avenue to observe subnanoclusters' morphological intuitively (Figure 1d). Especially for catalytic reaction under high temperature, size changes of SSCs is more concerned.

To date, most of the reviews about SSCs have focused on syntheses and applications.^[6,7,26–28] Although several articles

elaborate on the in situ techniques, authors are either concerned with multiple characterization methods other than XAS/SAXS^[27,29–32] or the focus is not on SSCs.^[28,33,34] Thus, in this article, we review the recent work on applying in situ XAS/SAXS to SSCs. We begin this review by describing the atomic structure variations of SACs obtained by Fourier transformed operando EXAFS spectra. The oxidation state of SACs under OCV and subsequent changes during the reaction process observed via in situ XAS are introduced. Meanwhile, the reversible transformation of SACs to subnanoclusters/nanoparticles is also be elaborated and discussed. We then extend the discussion to subnanoclusters, showing the combining use of in situ SAXS and in situ XAS to capture the size and valence changes simultaneously. Finally, the conclusions and outlook of modulating the SSCs and applying in situ XAS/SAXS in SSCs are highlighted.

2. In Situ XAS

2.1. Probing Atomic Structure

Single metal atom and coordinated atoms constitute the active site, determining the catalytic activity. Electronic structures of SACs and adsorption of intermediates are depended on the local geometric configuration of SACs.^[35] DFT calculations indicate that the electronic density of Co SACs can be tailored through regulating coordinated atoms.^[36] Chen et al. proposed that the coordinated S and P atoms can donate electrons to single-atom Fe centers, resulting in Fe is less positive, which helps weaken

the binding of adsorbed OH species.^[37] Han et al. prepared diatomic Pd–Cu sites in the PdN₂CuN₂ structure.^[38] The introduced Cu causes the shifting of partial density states of Pd and enhanced coupling between Pd and adsorbed N₂. The heteroatoms in the support that are not coordinated with single metal atoms also affect the oxidation state of SACs. The existence of S in the support results in the formation of Cu–N₄–C₈S₂ moieties, leading to Cu less positive than Cu in Cu–N₄–C₁₀.^[39] More importantly, the adsorbed species (hydroxyl, reactant, reaction intermediates, products, etc.) on SACs can change the chemical bond length between the metal atom and coordinated atoms and the corresponding coordination geometry. For instance, a new Ni–C bond is originated from adsorbed reaction intermediates on the nickel phthalocyanine under the CO₂ reduction reaction (CO₂RR) at –0.68 V.^[40] In some circumstances, the atomic configuration of SACs would undergo reconstruction during the catalytic reaction, rather than preserving static structure.

Fourier transform (FT) of EXAFS spectra is the most direct observation method to monitor the expand or contract behaviors of chemical bond that caused by species adsorption. Cao et al. proved the influence of hydroxyl adsorption on the local coordination environment of SACs under alkaline hydrogen evolution reaction (HER).^[25] The corresponding FT k³-weighted EXAFS spectra uncovered a shortening of Co–N bond upon chemical adsorption of hydroxyl at open circuit state. It is worth noting that the chemical bond length of Co–N remains unchanged during working conditions. Meanwhile, the Co–N bond intensity presents a tendency of decreases first and then increases under the open-circuit conditions and applied potential, respectively, revealing the change of coordination number of Co. Single Co atom experienced a local atomic structure rearrangement, changing from an isolated Co₁–N₄ site to a HO–Co₁–N₂ structure. Then H₂O–(HO–Co₁–N₂) moiety formed after potential is applied. The HO–Co₁–N₂ favors H₂O adsorption and dissociation with a low energy barrier. Operando XAS measurements captured atomic structure changes of ruthenium (Ru) SACs during the electrochemical nitrogen reduction reaction (NRR).^[41] The radial distance of the Ru–C(O) peak shifted from 1.58 to 1.51 Å in N₂-saturated K₂SO₄ solution under OCV compared with that in Ar-saturated K₂SO₄ solution, which might result from the Ru–N coordination (Figure 2a). After the potential is applied, the radial distance of the principal peak shifted to longer lengths of 1.56 Å, which suggests the distortion of Ru atoms caused by the electron density redistribution.

Zhong et al. pointed out that the peaks at 1.55 and 1.54 Å in FT-EXAFS spectra that were assigned as Zn–O bond and Cu–N bond, respectively, were not shifted during the CO₂RR.^[42] The Zn–O bond's peak intensity presents a negligible decrease, which is possibly due to the interaction of the reaction intermediates (*H, *COOH, *CO) and the ZnO₄ sites during the catalytic process. In contrast, Jiang et al. observed the shrinking of Cu–N bond length from 1.44 to 1.35 Å under catalytic conditions (Figure 2b).^[39] Meanwhile, compared with the ex situ sample, the coordination number changed from 4 to 5, attributing to the adsorption of oxygen ligand (OOH*, O*, or OH* intermediates) during the oxygen reduction reaction (ORR). Li et al. demonstrated that the non-planar ferrous Fe–N₄ moiety switches to an in-plane ferric Fe–N₄ moiety after axially bonded oxygen atom during the ORR (Figure 2c).^[21] The additional axial ligand will alter the energy level of d orbitals of SACs and the energy barrier for reactants binding. Besides, Fang et al. ascribed the appearance of one additional P–O bond under +0.15 V to adsorption of H₂O molecule on Pt.^[11] The XANES confirmed the increased structural disorder around the Pt atom. The FT k²-weighted EXAFS spectra provide more structure changes information. The Pt–C/N coordination number is reduced from 4 at OCV to 2 at –0.07 V, indicating Pt atoms are released from support. Pt SAC tends to be less coordinated with the N–C substrate during the HER. Yang et al. found the Ni–N bond in Ni–N₄ moiety slightly extended at –0.7 V compared with the sample at OCV, because of Ni atoms distorted out of the graphene plane after adsorption of CO₂.^[43]

Feng et al.^[44] and Jiang et al.^[45] observed Mn–N bond and Sb–N bond lengthened from 1.7 to 1.76 Å and 1.32 to 1.42 Å during the CO₂RR, respectively. However, Shang et al. found slightly shortened In–N bond (from 1.95 to 1.93 Å) at –0.65 V compared to that without applied potential.^[46] Chemical bond length changes during reaction become more complicated in two kinds of coordinated atoms for SACs. Shang et al. found the nearly unchanged Cu–S bond length and shortened Cu–N bond length in Cu–S₁N₃ moiety during the ORR compared with the ex situ sample.^[47]

2.2. Electronic Structure Evolution

The catalytic effect of SSCs is positively related to the oxidation state. Most SACs exist in cationic states, owing to the charge transfer from metal sites to support. Typically, the

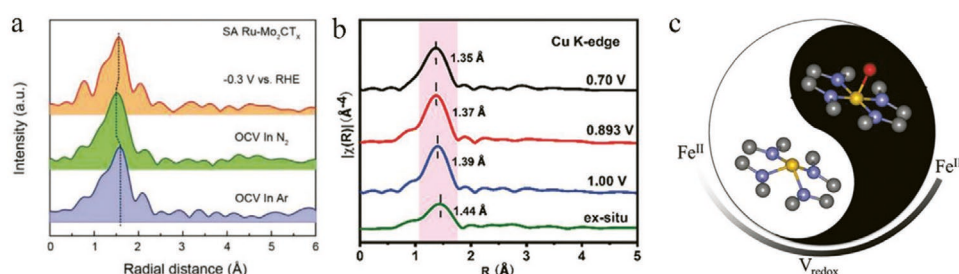


Figure 2. a) FT-EXAFS spectra of Ru under various conditions. Reproduced with permission.^[41] Copyright 2020, Wiley-VCH. b) k³-weighted FT-EXAFS spectra of Cu at ex situ, 1.0, 0.893, and 0.7 V. Reproduced with permission.^[39] Copyright 2019, Royal Society of Chemistry. c) The derived Fe–N switching behavior governed by the Fe²⁺/3⁺ redox potential. Reproduced with permission.^[21] Copyright 2016, Royal Society of Chemistry.

low-valence/metallic state SSCs are advantageous to electroreduction reactions, because more d-band electrons participate in the reaction, and catalysts bond more strongly with the reactants.^[11,48] The charge density and distribution of SACs dependent on the local coordination environment will affect the reactant adsorption and product desorption. Gu et al. demonstrated that faster CO₂ adsorption on Fe³⁺–N–C would lead to a lower onset overpotential than that on Fe²⁺–N–C moieties.^[49] Jiao et al. prepared Cu₁⁰–Cu₁x⁺ atom-pair catalyst.^[50] H₂O adsorbed on Cu₁x⁺, and CO₂ adsorbed on the neighboring Cu₁⁰ during the CO₂RR, promoting CO₂ activation. Note that the valence of SACs is usually not constant during catalytic reactions. Monitoring the oxidation state changes under realistic working conditions through in situ XAS is fundamental for revealing the actual active sites, understanding the reaction mechanism further, and offering guidance on catalysts design.

2.2.1. Open-Circuit Conditions

SACs are susceptible to the surrounding environments, especially when there is a lack of robust interaction between SACs and substrate. The local environment of SACs is probably affected by oxygen-containing groups or dissolved reactants in the electrolyte at OCV. Thus the influence of electrolyte on the charge state of SACs should be regarded.

For the HER, acidic electrolyte and acidic electrolyte exhibit different influence on the oxidation state of SACs. Pattengale

et al. found the reduction of 1T MoS₂ supported single-atom Ni²⁺ upon immersing in the acidic electrolyte at OCV.^[24] In contrast, compared with the dry sample, the change of oxidation state of Ni²⁺ SACs under acidic electrolyte condition is not apparent. In addition, the hydroxyl species or CO₂ molecules in the electrolyte are chemically adsorbed on the single-atom center, which will affect the valence of SACs. For instance, compared with the ex situ sample, the average valence of Co under the open-circuit conditions increases from +2.02 to +2.20, resulting from the adsorption of the hydroxyl group at the Co site.^[25] Yang et al. found that the oxidation state of Ni SACs in the KHCO₃ solution saturated with CO₂ is higher compared to the oxidation state of Ni in the KHCO₃ solution saturated with Ar under OCV.^[43] The increase in the oxidation state is attributed to the unpaired electron's delocalization, and the charge transfer from Ni to dissolved CO₂. Feng et al.^[44] and Shang et al.^[46] also proposed the charge transfer from low-valent SACs to the carbon 2p orbital of CO₂ with the formation of CO₂^{δ-} species, inducing the increased oxidation state of SACs (Figure 3a). Similarly, Liu et al. observed that the in situ formed low-valence Ni⁺ in Ar-saturated KHCO₃ solution would be oxidized back to Ni²⁺ by donating a lone pair electron in the 3d orbital after purging CO₂ molecules into the electrolyte.^[51] The Ru K-edge shifts to higher energy in N₂-saturated K₂SO₄ solution under OCV compared with that in Ar-saturated K₂SO₄ solution, resulting from the charge transfer from Ru SAs to the N 2p orbital of dissolved N₂.^[41] Besides, the oxygen dissolved in the electrolyte can oxidize the valence state of Mn SACs from +2 to +3.^[52]

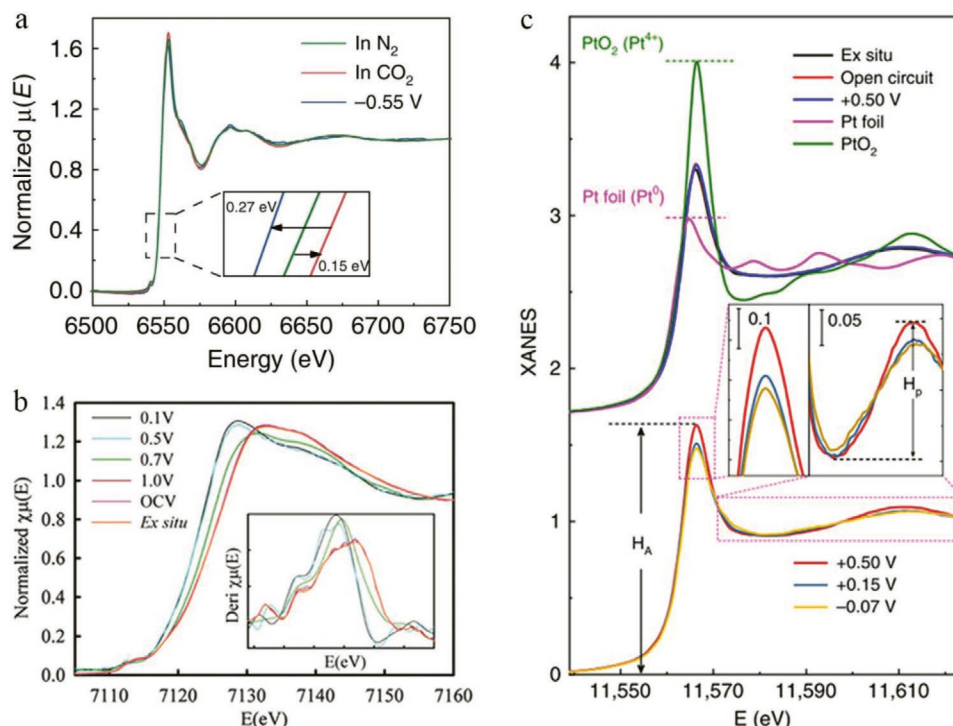


Figure 3. a) XANES spectra at the Mn K-edge of Mn–C₃N₄/CNT under various conditions. Reproduced with permission.^[44] Copyright 2020, Springer Nature. b) Ex situ and in situ XANES spectra of Fe SACs. Reproduced with permission.^[21] Copyright 2016, Royal Society of Chemistry. c) XANES spectra at different applied voltages from the open-circuit conditions to –0.07 V during the HER. The inset shows the enlarged white-line peak, and postedge XANES region. Reproduced with permission.^[11] Copyright 2020, Springer Nature.

In other studies, compared with ex situ samples, the oxidation state of SACs did not undergo any changes after being immersed in electrolyte where no voltage was applied. For example, Gu et al. proved the unchanged valence of Fe SACs at OCV.^[49] Li et al. obtained Fe K-edge XANES spectra of in situ electrode at open circuit conditions, which are similar to that of the ex situ electrode, indicating the unvaried oxidation state of Fe (Figure 3b).^[21] Besides, Fang et al. highlighted that the prepared Pt SAC is structurally stable, and no chemical reactants are adsorbed in the electrolyte at OCV (Figure 3c).^[11] The Pt SAC maintains its original valence state until the voltage is applied.

2.2.2. Working Conditions

Identifying active centers by in situ XAS during realistic reaction process is advantageous to reveal the reaction mechanism. The as-prepared SACs usually do not act as active sites. When voltage is applied, the SACs-support interaction will be weakened or strengthened, along with charge transfer behaviors between SACs and coordinated atoms. The XANES of Ru SACs^[41] and Fe SACs^[53] moved toward lower energy during the NRR process, suggesting N₂ molecules donate electrons to unoccupied d orbitals of metal atoms. Li et al. noticed that the average oxidation number of iridium (Ir) SACs manifested a conspicuous potential-dependent variation.^[54] From 0 to 0.64 V, 5d band occupancy of Ir became higher, because of electron transfer from formic acid to Ir during the formic acid oxidation reaction. Malta et al. found that the gold (Au) L₃-edge XANES spectrum's white line intensity decreased steadily to a stable value after an initial increase under acetylene hydrochlorination reaction.^[55] As Au(I) was oxidized to predominantly Au(III) and then moved back to Au(I), the catalytic performance has shown a decrease first and then increase, indicating the presence of Au(I) is beneficial for the reaction.

The evolution of the oxidation state of SACs during the HER and the CO₂RR has been explored. The absorption edge position of Co shifts toward higher energy during the HER in 1.0 M KOH, implying an increase of the Co oxidation state.^[25] Jiang et al. observed an increase of white line's peak intensity of antimony (Sb) K-edge XANES and the absorption edge shifts to higher energy during the CO₂RR, which attribute to the charge transfer from low-valent Sb^{δ+} to CO₂ molecule.^[45] Differentiating from the oxidized SACs during the working conditions mentioned above, Gu et al. demonstrated the Fe³⁺ transformed into Fe²⁺ after −0.5 V during the CO₂RR.^[49] The decreased catalytic activity for generating CO after −0.5 V indicates Fe³⁺ is the catalytic site. However, Shang et al. considered the reduced indium (In) SACs at −0.65 V as catalytic center for the CO₂RR with high selectivity of formate.^[46] When a potential of −0.65 V was applied, the In K-edge shifted to lower energy, suggesting that In SACs return to a low valence state. Feng et al. observed the same valence evolution of manganese (Mn) SACs during the CO₂RR.^[44] The reduced Mn SACs as active site show the high CO Faradaic efficiency. Fang et al. revealed that the white-line intensity of Pt L₃-edge XANES decreased during the HER in 1.0 M KOH electrolyte, implying the average oxidation state of cationic Pt is close to zero valence (Figure 3c).^[11]

Several works have disclosed the valence variations of SACs through in situ XAS during the ORR. Jia et al.^[56] and Li et al.^[21] found the Fe²⁺/Fe³⁺ redox transition in 0.1 M HClO₄ electrolyte. When the applied potential is increased from 0.1 to 1.0 V, the Fe K-edge shifts toward the higher energy (Figure 3b). The low valent Fe²⁺–N₄ moieties transformed into oxidized Fe³⁺–N₄ moieties with the adsorption of *OH during the water activation process. Similarly, Xiao et al. reported the in situ reduced non-planar HO–*Fe(2+)–N₄ moieties as ORR's active site, which is then oxidized to a pentacoordinate O_x–Fe³⁺–N₄ at potentials that above the Fe²⁺/Fe³⁺ redox potential.^[57] In situ XAS collects a positive shift in Fe K-edge XANES. Compared with the increased oxidation state of Fe SACs during the ORR in acid electrolyte, the decreased valence of SACs was observed in the alkaline electrolyte. Cheng et al. uncovered that the valence of single-atom Fe gradually decreased as the applied potential was from 1.0 to 0.3 V during the ORR.^[37] Similarly, with the potential, scanned from 1.05 to 0.75 V, the peak position of Cu K-edge absorption spectra shifted toward the low energy side, along with intensity reduction of white line peak, which means that the oxidation state of Cu SACs has been decreased (Figure 4a,b).^[47] Jiang et al. also demonstrated that the average valence state of Cu dropped from 1.59 to 1.09 as the potential decreased from 1.00 to 0.70 V.^[39] In these two studies, low-valence Cu (+1) in the asymmetric Cu–S₁N₃ moiety^[47] and Cu (+1)–N₄–C₈S₂ atomic interface moiety^[39] worked as active sites for the ORR. The operando Mn K-edge XAS experiment shows the same trend. The valence state of Mn SACs decreased from +3 to a lower value as the applied potential decreased from 0.9 to 0.3 V, corresponding to increased ORR overpotential.^[52]

Unlike the increased oxidation state of Fe SACs, the operando XANES of Co SACs were maintained throughout the ORR in an acid medium (Figure 4c,d).^[58] The authors believe that binding between Co–N–C moieties and O₂ is too weak to reduce O₂ effectively. Liu et al.^[51] and Jiang et al.^[59] discovered that during electrolysis CO₂ reduction, the Ni K-edge XANES spectra are generally similar in CO₂-saturated KHCO₃ solution under different applied potentials. Sun et al. put forward that single-atomic cobalt catalyst retains a stable charge state during the catalytic hydrogen evolution process.^[60] Yao et al. demonstrated that the oxidation state of Ru SAC was almost unchanged upon changing the applied potential during oxygen evolution reaction (OER).^[61] Zhong et al. considered that the unvaried oxidation state of single-atom dispersed zinc (Zn) under the CO₂RR can be attributed to a full 3d electron shell of Zn (II).^[42]

Even under the same catalytic reaction, the valence changes of SACs during the reaction vary with the different SACs reported. The synthesis strategy determines the degree of interaction between the SAC and the carrier, which will affect the oxidation state changes of the SAC under open circuit and working conditions. Moreover, researchers should collect as many XAS at different potentials as possible to convey the results intuitively and accurately.

2.3. SACs to Clusters/Nanoparticles Transformation

Catalysts experience irreversible nanoclustering,^[62] morphology variation,^[63] phase/structural transformation^[64–66] during

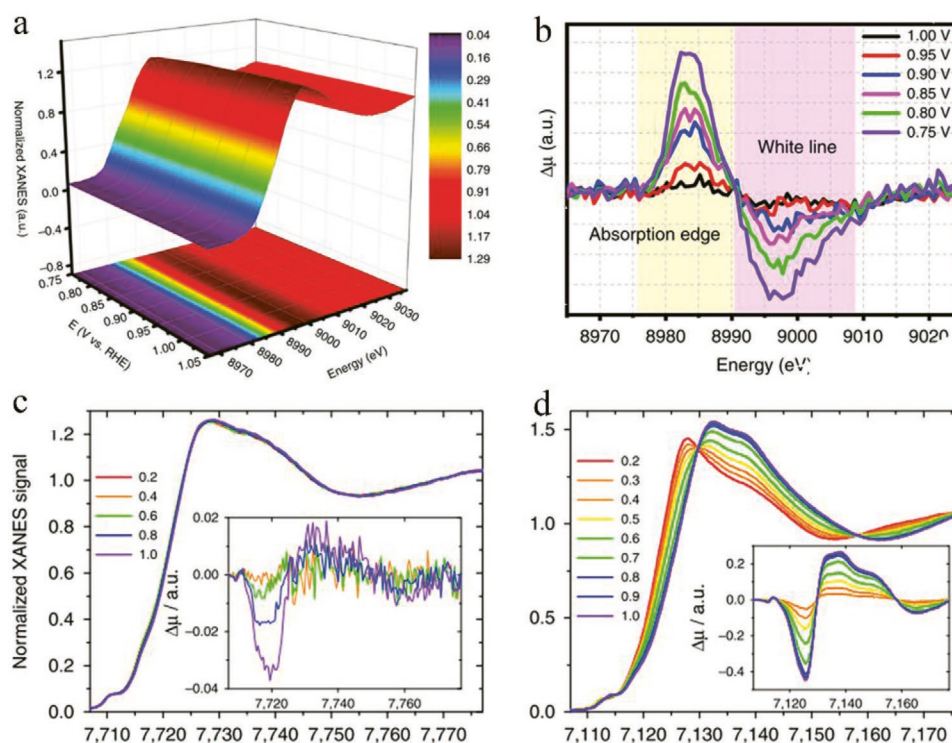


Figure 4. a) In situ Cu K-edge XANES spectra at various potentials during the ORR catalysis and b) differential $\Delta\mu$ XANES spectra obtained by subtracting the normalized spectrum at every potential to the spectrum recorded at 1.05 V. Reproduced with permission.^[47] Copyright 2020, Springer Nature. Operando XANES spectra in 0.5 M H_2SO_4 of c) $\text{Co}_{0.5}$ and d) $\text{Fe}_{0.5}$. Insets are differential $\Delta\mu$ XANES spectra obtained by subtracting the normalized spectrum at every potential to the spectrum recorded at 0.2 V. Reproduced with permission.^[58] Copyright 2020, Springer Nature.

working conditions. SACs typically remain the initial atomic dispersed state after catalysis. Remarkably, in some cases, single atoms to clusters/nanoparticles transformation during the electrocatalytic reaction is observed by in situ synchrotron XAS.

Karapinar et al. revealed a reversible transformation between ionic Cu SACs and metallic Cu nanoparticles during the CO_2 reduction process.^[23] The oxidation state of Cu decreased from +2 to 0, which demonstrates the metallic Cu nanoparticle as the catalytically active site for CO_2 electroreduction (Figure 5a). FT-EXAFS spectra recorded the decreased intensity of Cu–N bond as the potential applied from OCV to –1.2 V (Figure 5b). Meanwhile, the presence of Cu–Cu bond illustrates the aggregation of Cu SACs. It should be noted that the post-electrolysis Cu nanoparticles were converted back to single atoms after exposure to air for 10 h. This reversible conversion stands out the necessity of the application of in situ characterization technologies to study active sites. Subsequently, Xu et al. also demonstrated this reversible transition.^[22] As shown in Figure 5c,d, the Cu K-edge XANES spectra shifts to the lower energy side with the presence of Cu–Cu bond at –0.7 V, denoting the existence of metallic Cu_n ($n = 3$ and 4) clusters. The electron transferred from carbon substrate to isolated Cu^{2+} under the potential operating results in the formation of metallic Cu, which serves as the active site to adsorb dissolved CO_2 . By the way, the unstable Cu_n can be oxidized into atomically dispersed cations under postreaction conditions (Figure 5d). Based on the operando measurements, the authors proposed a hypothesized reaction mechanism (Figure 5e). Maurer et al. further clarified

the single-atoms to clusters reversible transformation of Pt single sites (Pt-SS) supported on cerium oxide (CeO_2) during the CO oxidation reaction via operando high-energy-resolution fluorescence detected XAS.^[67] Oxygen is desorbed from Pt^{4+} sites below 150 °C, resulting in the formation of Pt^{2+} . Up to 150 °C, Pt species undergo further reduction and restructure to $\text{Pt}^{\delta+}$ –CO. With the breaking of Pt–O–Ce bonds at the higher reaction temperature, $\text{Pt}_x^{\delta+}$ clusters as active sites appeared, consistent with the increased CO conversion. The in situ formed $\text{Pt}_x^{\delta+}$ clusters experience reoxidizing and redispersing during cooling, generating the initial Pt-SS state.

The stability of SACs also depends on the electrolyte in electrocatalytic reactions. Pattengale et al. reported distinct transformation behaviors of Ni SACs in acidic electrolyte and alkaline electrolyte during the HER.^[24] Atomically dispersed Ni is predominantly coordinated to S with a smaller contribution of O in the as-prepared dry sample. Under acidic conditions, a shifting of Ni K-edge in XANES toward lower energy is observed at precatalytic (0 V) and catalytic (–0.76 V) potentials. The valence of Ni changes from 2+ to 1+ without a change of atomic structure (Figure 6a). In alkaline media, upon immersion in alkaline electrolytes at OCV, a conspicuous second-shell scattering that originates from the Ni–Ni bond is observed. Meanwhile, compared with the as-prepared sample, the first-shell peak shifts to smaller position at OCV and 0 V, due to Ni is principally coordinated with O by the formation of Ni–O–Ni moieties. The coordination number of Ni is decreased under applied catalytic potential (–0.76 V), concurrent with the formation of metallic

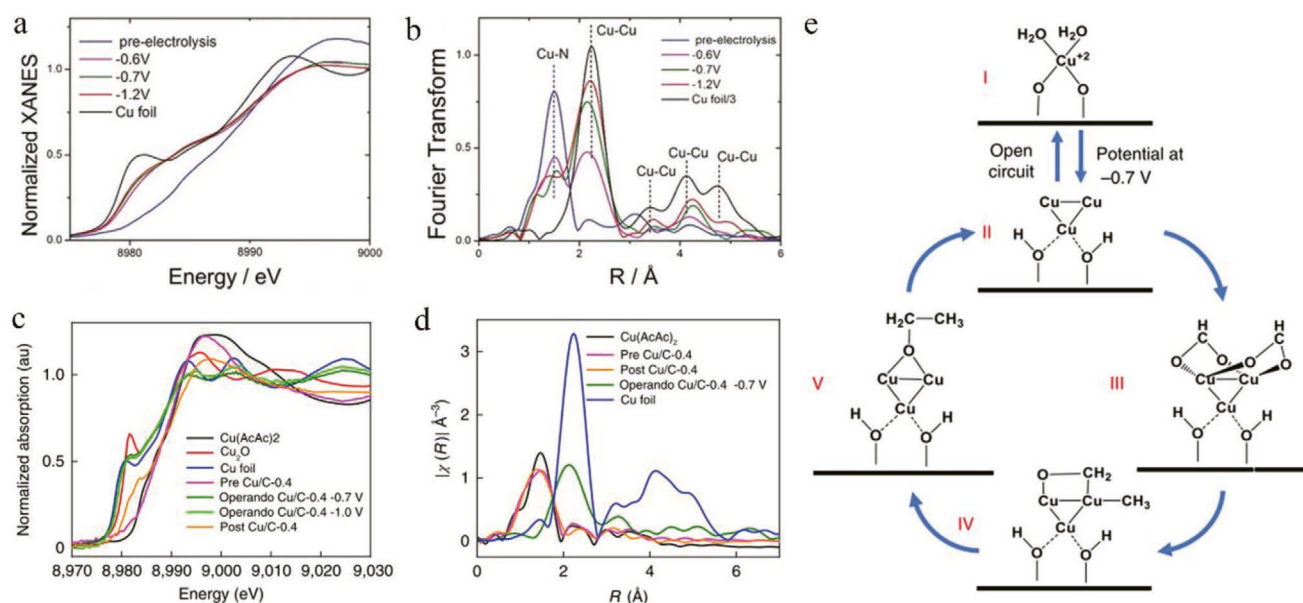


Figure 5. a) In situ Cu K-edge XANES spectra. b) Fourier transform of the experimental EXAFS spectra of Cu. Reproduced with permission.^[41] Copyright 2019, Wiley-VCH. c) In situ Cu K-edge XANES spectra. d) Fourier transform of k^2 -weighted χ function in R space of the catalysts. e) The hypothesized reaction mechanism during the CO₂RR. Reproduced with permission.^[22] Copyright 2020, Springer Nature.

Ni clusters. Besides, the post-catalysis ex situ XAS on Ni K-edge indicates a reversible transformation from catalytically active metallic Ni species to initial high-valence NiS_xO_y moieties. Based on the results, the authors proposed respective active sites in acidic and alkaline electrolyte (Figure 6b).

From the above discussion, we note that the as-prepared cationic state SACs are reduced to the metallic state, which means less coordinated with the substrate, resulting in the formation of clusters/nanoparticles. However, agglomerated SAs can be oxidized into initial high valence state at postcatalysis conditions. Thus, the robust interaction between SACs and support is essential to achieve a stable atomic structure during working conditions. For example, Peterson et al. observed the aggregation of atomically dispersed Pd on alumina during the CO oxidation reaction.^[68] The EXAFS data show a decrease in the peak intensity of Pd–O first-shell accompanied by the emerging Pd–metal peak, reflecting the growth of Pd-metal. In contrast, Pd preserves the single atom state when there is lanthanum (La) on the substrate surface. Even though La can slow the catalyst sintering rate, subnanometer clusters still appeared at higher reaction temperatures, with apparent inferior catalysis

activity. Based on the discussion mentioned above, utilizing in situ SAXS to study the transformation from SACs to clusters during working conditions is significant for size-dependent performance.

3. In Situ SAXS

SAs/clusters are subjected to aggregate into larger sizes or nanoparticles during the reaction or synthesis process without sufficient support. Besides, the oxidation state of the catalyst is dependent on the size. For example, the Cu₂₀ cluster possesses the lowest charge state among the Cu₂₀, Cu₄, and Cu₃ clusters.^[69] Wei et al. proved more positively charged Pt SACs compared with Pt clusters and nanoparticles.^[70] Similarly, Maurer et al. demonstrated predominantly +2 oxidation state of Pt single sites.^[67] In contrast, the oxidation state of Pt is about 0 in Pt nanoparticles. To simultaneously track the size and oxidation state of working catalysts, in situ SAXS and in situ XANES characterizations are highly indispensable.^[71,72]

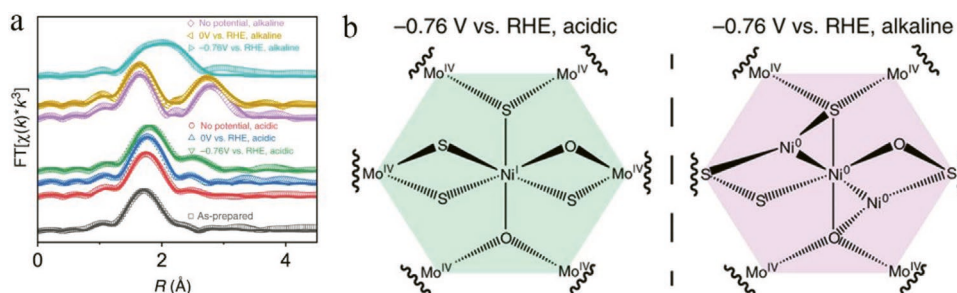


Figure 6. a) FT-EXAFS spectra of Ni SACs at different electrolytes and potentials. b) The proposed Ni@1T-MoS₂ active species. The active species under acidic (left) and alkaline (right) conditions. Reproduced with permission.^[24] Copyright 2020, Springer Nature.

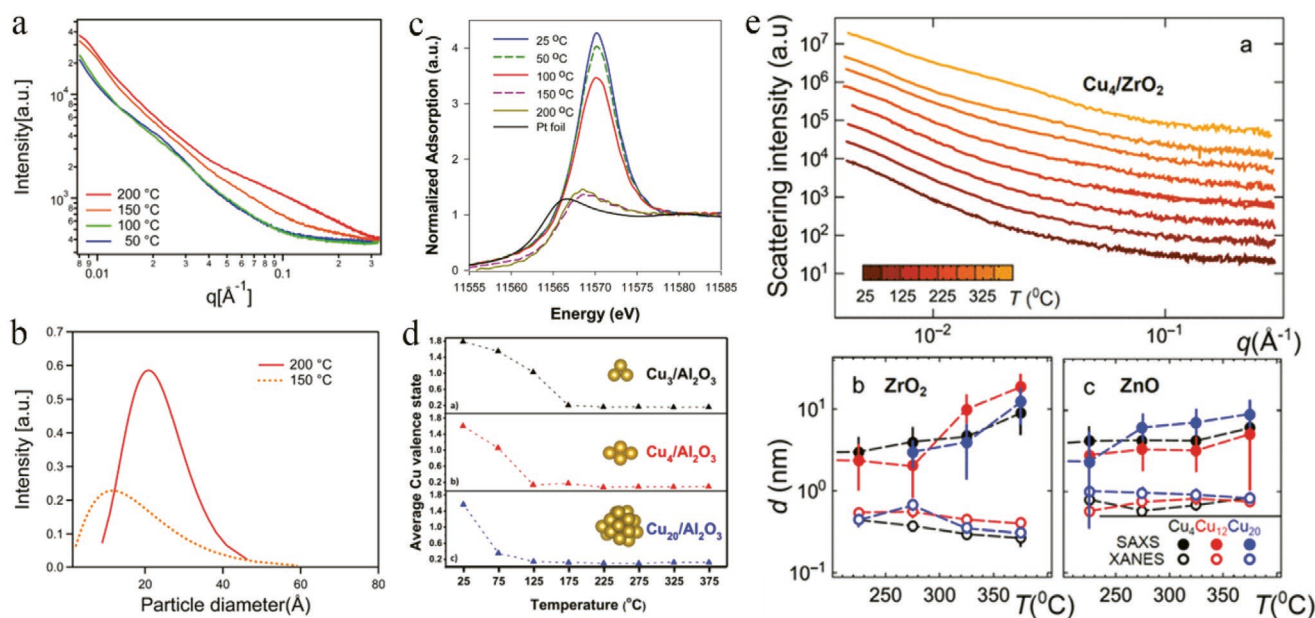


Figure 7. a) GISAXS intensity change of $\text{Pt}_{24}/\text{SiO}_2/\text{Si}$ sample during the heating cycle. b) Fitted particle size distributions. c) XANES, normalized to the intensity above the edge, for a soft-landed $\text{Pt}_{24}/\text{SiO}_2/\text{Si}$ sample at different annealing temperature. Reproduced with permission.^[73] Copyright 2017, American Chemical Society. d) The average Cu charge state with increasing reaction temperatures. Reproduced with permission.^[69] Copyright 2017, American Chemical Society. e) Temperature-dependent GISAXS data for Cu_4 clusters on ZrO_2 . Reproduced with permission.^[74] Copyright 2018, American Chemical Society.

Dai et al. revealed the correlation between the size and oxidation state of Pt clusters via operando grazing-incidence SAXS (GISAXS) and grazing-incidence XAS.^[73] As the $\text{Pt}_{24}/\text{SiO}_2/\text{Si}$ sample was calcinated from 50 to 200 °C in H_2 , there is a significant signal enhancement in the q range around 0.1 \AA^{-1} at 150 and 200 °C, respectively (Figure 7a). The fitted particle size distributions show obvious cluster agglomeration (Figure 7b). Simultaneously, the white line intensity of Pt L_3 -edge XANES gradually decreases, approaching the intensity for Pt foil (Figure 7c). After excluding the possibility of Pt reduction during heating by XPS, they concluded that sintered small nanoparticles display more bulk-like electronic properties than the initial clusters. Yang et al. concluded that the size and oxidation state determine the CO_2 hydrogenation activity of Cu clusters.^[69] In situ GISAXS experiments of Cu_n ($n = 20, 4, 3$) clusters show no aggregates during the reaction process, indicating the sintering resistant property of clusters on Al_2O_3 . As the reaction temperature increases, the average Cu valence state decreases rapidly first and then remains stable (Figure 7d). Besides, the CO_2 reduction temperature decreases with increasing cluster size. Timoshenko et al. studied electronic structure and size variations of Cu_4 , Cu_{12} , and Cu_{20} clusters soft-landing on different oxide substrates (ZrO_2 and ZnO).^[74] The agglomeration of Cu clusters can be detected by the temperature-dependent GISAXS (Figure 7e). It is worth noting that, compared with the ZrO_2 support, the size changes for clusters on the ZnO support are less pronounced in the high-temperature range, which implies the possibility of significant agglomeration of the ZnO -supported clusters in the low-temperature range. Upon heating, Cu K-edge XANES spectra show the downward shift of the absorption edge position and the decrease of white line intensity, indicating that Cu clusters are rapidly reduced.

4. Conclusions and Outlook

The urgent demand for designing SSCs with high catalytic activity and high selectivity has prompted researchers to focus on active sites during working conditions. Compared with other characterization techniques, operando XAS and operando SAXS exhibit unparalleled advantages in exploring oxidation state/local atomic structure changes of SACs and cluster size evolutions, respectively.

As shown in Table 1, we summarized the changes of SACs at OCV and working conditions. The electron transformation between the hydroxyl groups or adsorbed reactants and SACs affects the oxidation state/atomic structure of SACs. Moreover, identifying the relationship between product selectivity and valence state during some catalysis reactions by in situ XAS is meaningful. Additionally, in consideration of the size-dependent catalytic activity, researchers should combine in situ SAXS to monitor subnanoclusters' size changes under working conditions. Based on the above discussion, the inspirations for SSCs design and future direction of application of operando XAS/SAXS in SSCs are summarized as follows:

4.1. Adjusting Electronic States

Compared with most SACs sustain oxidation state, subnanoclusters have the advantage of less positively charged constituent atoms. Reduced clusters act as active sites in some reduction reactions.^[22] In contrast, high-valence metal atoms are beneficial for some electrooxidation catalytic reactions. For instance, Zheng et al.^[75] and Zhang et al.^[76] constructed high-valence metal sites with enhanced water oxidation ability. Lee

Table 1. A brief summary of the SACs changes at OCV and working conditions.

Reaction	Materials	Open-circuit voltage	Working conditions		Ref
			Oxidation state	Atomic structure	
CO ₂ RR	Fe ³⁺ –N–C	No obvious changes	Fe ³⁺ is reduced to Fe ²⁺	N/A	[49]
	Ni–NG	N/A	No obvious changes	N/A	[59]
	Ni–CNT–CC	N/A	No obvious changes	N/A	[51]
	A–Ni–NG	An increase of Ni oxidation state, appearance of new Ni–C bond	An increase of Ni oxidation state	Expansion of Ni–N bond	[43]
	Mn–C ₃ N ₄ /CNT	An increase of Mn oxidation state, coordination number is increased slightly	Shift back to lower oxidation state	Lengthening of Mn–N bond, coordination number is increased slightly	[44]
	Sb SAs/NC	N/A	An increase of Sb oxidation state	Extended Sb–N bond	[45]
	In–SAs/NC	An increase of In oxidation state	A decrease of Ni oxidation state	Shortened In–N bond length	[46]
	Cu/C-0.4	N/A	Ionic Cu is reduced to metallic Cu	Transformation from SAs to clusters	[22]
	Cu _{0.5} NC	N/A	Cu ²⁺ is reduced to metallic Cu	Transformation from SAs to nanoparticles	[23]
ORR	FePhenMOF–ArNH ₃	No obvious changes	An increase of Fe oxidation state (0.1–1.0 V)	Increased coordination number	[21]
	Fe–SAs/NPS–HC	N/A	A decrease of Fe oxidation state (1.0–0.3 V)	N/A	[37]
	Fe–N–C	N/A	Fe ²⁺ –N ₄ oxidized to a pentacoordinate O _x –Fe ³⁺ –N ₄	N/A	[57]
	Cu–SA/SNC	N/A	A decrease of Cu oxidation state (1.0–0.7 V)	Shrinking of Cu–N bond	[39]
	S–Cu–ISA/SNC	N/A	A decrease of Cu oxidation state (1.0–0.75 V)	Shrinking of Cu–N bond	[47]
	Mn–SAs/CN	An increase of Mn oxidation state	A decrease of Mn oxidation state (0.9–0.3 V)	N/A	[52]
OER	Ru ₁ –Pt ₃ Cu	N/A	No obvious changes	Increased coordination number	[61]
HER	Co ₁ /PCN	An increase of Co oxidation state, increased peak intensity, decreased mean bond length	A decrease of Co valence state	Increased coordination number	[25]
	CoSAs/HOPNC	N/A	No obvious changes	No obvious changes	[60]
	Pt ₁ /N–C	No obvious changes	Pt site is reduced toward metallic state	Coordination number is decreased from 4 to 2	[11]
	Ni@1T–MoS ₂	A reduce of Ni oxidation state	A reduce of Ni oxidation state	No obvious changes	[24]
	Acidic electrolyte Alkaline electrolyte	Appearance of Ni–Ni bond, transformation from Ni–S to Ni–O bond	Ni ²⁺ was reduced to metallic Ni	Coordination number is decreased, only exist Ni–Ni bond	
NRR	SA Ru–Mo ₂ CTX	An increase of Ru oxidation state, Shrinking of Ru–C(O) bond	A reduce of Ru oxidation state	Lengthening of Ru–C(O) bond	[41]
	Fe _{SA} –N–C	N/A	A reduce of Fe oxidation state	N/A	[53]

et al. pointed out that the oxidized nature of the under-coordinated cobalt atoms in clusters substantially decreases the cyclohexene species' binding energy during oxidative dehydrogenation of cyclohexane.^[77] Besides, the synergistic effect of two different valence states at the same metal site exhibits improved catalytic activity. For example, the coexistence of Cu(I) and Cu⁰ species leads to an increase in ethanol selectivity during the CO₂RR by enhancing CO dimerization.^[78–80]

4.2. Modulating Local Coordination Environment

Modulating the local coordination environment (coordinated atoms, coordination numbers, etc.) of SSCs helps improve catalytic activity. The coordinated atoms act as anchoring sites to stabilize the SSCs and play an essential role in optimizing the electronic structure and adjusting adsorption–desorption strength toward active sites' reaction species. For instance, Han

et al. introduced axially bonded chlorine into the Fe–N₄ planar structure to adjust the active center's electronic structure and optimize the binding strength of O₂, leading to an enhanced electrochemical performance of the ORR in alkaline media.^[81] In addition to nonmetallic heteroatoms, the extra single metal sites in the support can also tune the active center's local coordination environment. The charge transfer from Ni atom to Fe atom through the conjugated π bond of graphene is thermodynamically beneficial to the 4e[−] ORR.^[82] The formation of an atom dimer between two single metal sites demonstrates another way to adjust the SACs active center's coordination environment. Lu et al. designed a ZnCoN₆ structure with isolated zinc-cobalt atomic pair.^[83] Co as active center shows the enhanced binding ability of O₂ compared with that in Co–N₄ structure, which facilitates the cleavage of O–O bond during the ORR.

4.3. SSCs-Support Interactions

The effect of support is stabilizing SSCs on the substrate and regulating the d-band center of the metal site. High loading of SACs have higher demand for structural stability.^[84–87] Although the strong interaction strength prevents aggregation, excessively strong interaction impedes the self-adjustment of active sites' coordination environment.^[88] Thus, the stability and catalytic activity should be optimized at the same time. Considering each support's different characteristics (carbon, metal, metal oxides/sulfides, etc.), it is a promising approach to adjust the electronic state of SSCs by loading on different supports or modifying properties of supports.^[89–91] For example, single Pt atoms on TiC exhibit higher activity, selectivity, and stability for H₂O₂ production than that on TiN.^[13] In addition, introducing more Pt in Pt–Cu alloy substrate can engineer the electronic structure of the supported Ru SACs, allowing optimized binding of oxygen species and better resistance to over-oxidation and dissolution.^[61] Support effect is also reflected in the stability of SSCs. The dissolution of S ligands from the carbon support matrix leads to Pt SACs becoming more prone to agglomeration.^[10]

4.4. Identifying Active Sites

The principal objective of in-situ XAS/SAXS study is to identify the active site under real-time working conditions. This is crucial for studying catalytic mechanisms and guiding the synthesis of the optimized SSCs. Generally, SSCs experience oxidation state/atomic structure changes under OCV and working conditions compared to the prepared samples. The adsorbed hydroxyl species/reactant/reaction intermediates on SSCs also affect the coordination environments. The influence of the electrolyte on SACs at OCV should not be ignored.

4.5. Combining Operando Soft XAS

Compared with hard XAS (>5 keV), soft XAS (<1 keV) is more surface sensitive, which is widely used to study the chemical

state of nonmetallic elements (such as K-edges of C, N, O, and L-edge of S).^[39,92,93] Metal L-edge spectra describe the transitions of 2p electrons to unfilled d-orbitals.^[94] Oxidation state changes of metal sites will be better revealed by exploring the L-edge of transition metal by in situ soft XAS. Even though complicated measuring environments limit the application of in situ soft XAS to catalytic reactions, in situ soft XAS shows a bright future to study the chemical state of SSCs and the coordinated atoms.

Acknowledgements

T.L. is thankful for the support from the U.S. National Science Foundation (Grant No. 1924574). This research used resources of the Advanced Photon Source, a U.S. Department of Energy (DOE) Office of Science User Facility, operated for the DOE Office of Science by Argonne National Laboratory under Contract No. DE-AC02-06CH11357.

Conflict of Interest

The authors declare no conflict of interest.

Keywords

in situ techniques, operando XAS/SAXS, single-atom catalysts, subnanoclusters

Received: December 1, 2020

Revised: January 21, 2021

Published online: February 12, 2021

- [1] Z. Li, D. He, X. Yan, S. Dai, S. Younan, Z. Ke, X. Pan, X. Xiao, H. Wu, J. Gu, *Angew. Chem., Int. Ed.* **2020**, *59*, 18572.
- [2] Y. Chen, J. Lin, L. Li, B. Qiao, J. Liu, Y. Su, X. Wang, *ACS Catal.* **2018**, *8*, 859.
- [3] X. Han, X. Ling, Y. Wang, T. Ma, C. Zhong, W. Hu, Y. Deng, *Angew. Chem., Int. Ed.* **2019**, *58*, 5359.
- [4] X.-F. Yang, A. Wang, B. Qiao, J. Li, J. Liu, T. Zhang, *Acc. Chem. Res.* **2013**, *46*, 1740.
- [5] L. Fang, Z. Feng, L. Cheng, R. E. Winans, T. Li, *Small Methods* **2020**, *4*, 2000315.
- [6] Z. Song, L. Zhang, K. Doyle-Davis, X. Fu, J. L. Luo, X. Sun, *Adv. Energy Mater.* **2020**, *10*, 2001561.
- [7] Z. Li, S. Ji, Y. Liu, X. Cao, S. Tian, Y. Chen, Z. Niu, Y. Li, *Chem. Rev.* **2020**, *120*, 623.
- [8] L. Zhang, D. Liu, Z. Muhammad, F. Wan, W. Xie, Y. Wang, L. Song, Z. Niu, J. Chen, *Adv. Mater.* **2019**, *31*, 1903955.
- [9] Y. Li, J. Wu, B. Zhang, W. Wang, G. Zhang, Z. W. Seh, N. Zhang, J. Sun, L. Huang, J. Jiang, J. Zhou, Y. Sun, *Energy Storage Mater.* **2020**, *30*, 250.
- [10] F. D. Speck, M. T. Y. Paul, F. Ruiz-Zepeda, M. Gatalo, H. Kim, H. C. Kwon, K. J. J. Mayrhofer, M. Choi, C. H. Choi, N. Hodnik, S. Cherevko, *J. Am. Chem. Soc.* **2020**, *142*, 15496.
- [11] S. Fang, X. Zhu, X. Liu, J. Gu, W. Liu, D. Wang, W. Zhang, Y. Lin, J. Lu, S. Wei, Y. Li, T. Yao, *Nat. Commun.* **2020**, *11*, 1029.
- [12] B. Qiao, A. Wang, X. Yang, L. F. Allard, Z. Jiang, Y. Cui, J. Liu, J. Li, T. Zhang, *Nat. Chem.* **2011**, *3*, 634.
- [13] S. Yang, Y. J. Tak, J. Kim, A. Soon, H. Lee, *ACS Catal.* **2017**, *7*, 1301.
- [14] A. Kodre, I. Arčon, J. P. Gornilšek, *Acta Chim. Slov.* **2004**, *51*, 1.

- [15] J. Yano, V. K. Yachandra, *Photosynth. Res.* **2009**, 102, 241.
- [16] F. M. de Groot, *Chem. Rev.* **2001**, 101, 1779.
- [17] C. H. van Oversteeg, H. Q. Doan, F. M. de Groot, T. Cuk, *Chem. Soc. Rev.* **2017**, 46, 102.
- [18] K. Qian, R. E. Winans, T. Li, *Adv. Energy Mater.* **2021**, 11, 2002821.
- [19] T. Li, A. J. Senesi, B. Lee, *Chem. Rev.* **2016**, 116, 11128.
- [20] R. E. Winans, S. Vajda, B. Lee, S. J. Riley, S. Solnke, G. Y. Tikhonov, N. A. Tomczyk, *J. Phys. Chem. B* **2004**, 108, 18105.
- [21] J. Li, S. Ghoshal, W. Liang, M.-T. Sougrati, F. Jaouen, B. Halevi, S. McKinney, G. McCool, C. Ma, X. Yuan, Z.-F. Ma, S. Mukerjee, Q. Jia, *Energy Environ. Sci.* **2016**, 9, 24182.
- [22] H. Xu, D. Rebolgar, H. He, L. Chong, Y. Liu, C. Liu, C.-J. Sun, T. Li, J. V. Muntean, R. E. Winans, D.-J. Liu, T. Xu, *Nat. Energy* **2020**, 5, 623.
- [23] D. Karapinar, N. T. Huan, N. R. Sahraie, J. Li, D. Wakerley, N. Touati, S. Zanna, D. Taverna, L. H. G. Tizei, A. Zitolo, F. Jaouen, V. Mougél, M. Fontecave, *Angew. Chem., Int. Ed.* **2019**, 131, 15242.
- [24] B. Pattengale, Y. Huang, X. Yan, S. Yang, S. Younan, W. Hu, Z. Li, S. Lee, X. Pan, J. Gu, J. Huang, *Nat. Commun.* **2020**, 11, 4114.
- [25] L. Cao, Q. Luo, W. Liu, Y. Lin, X. Liu, Y. Cao, W. Zhang, Y. Wu, J. Yang, T. Yao, S. Wei, *Nat. Catal.* **2018**, 2, 134.
- [26] S. Ji, Y. Chen, X. Wang, Z. Zhang, D. Wang, Y. Li, *Chem. Rev.* **2020**, 120, 11900.
- [27] X. Li, X. Yang, J. Zhang, Y. Huang, B. Liu, *ACS Catal.* **2019**, 9, 2521.
- [28] J. Timoshenko, B. R. Cuenya, *Chem. Rev.* **2021**, 121, 882.
- [29] X. Li, S. Wang, L. Li, Y. Sun, Y. Xie, *J. Am. Chem. Soc.* **2020**, 142, 9567.
- [30] A. D. Handoko, F. Wei, J. B. S. Yeo, Z. W. Seh, *Nat. Catal.* **2018**, 1, 922.
- [31] J. Lia, J. Gong, *Energy Environ. Sci.* **2020**, 13, 3748.
- [32] J. Yang, W. Li, D. Wang, Y. Li, *Small Struct.* **2020**, 2000051, <https://doi.org/10.1002/sstr.202000051>.
- [33] M. Wang, L. Árnadóttir, Z. J. Xu, Z. Feng, *Nanomicro Lett.* **2019**, 11, 47.
- [34] J. Park, J. Cho, *Angew. Chem., Int. Ed.* **2020**, 59, 15314.
- [35] J. Yang, W. Li, D. Wang, Y. Li, *Adv. Mater.* **2020**, 32, 2003300.
- [36] Y. Chen, R. Gao, S. Ji, H. Li, K. Tang, P. Jiang, H. Hu, Z. Zhang, H. Hao, Q. Qu, X. Liang, W. Chen, J. Dong, D. Wang, Y. Li, *Angew. Chem., Int. Ed.* **2020**, 59, 2.
- [37] Y. Chen, S. Ji, S. Zhao, W. Chen, J. Dong, W. C. Cheong, R. Shen, X. Wen, L. Zheng, A. I. Rykov, S. Cai, H. Tang, Z. Zhuang, C. Chen, Q. Peng, D. Wang, Y. Li, *Nat. Commun.* **2018**, 9, 5422.
- [38] L. Han, Z. Ren, P. Ou, H. Cheng, N. Rui, L. Lin, X. Liu, L. Zhuo, J. Song, J. Sun, J. Luo, H. L. Xin, *Angew. Chem., Int. Ed.* **2020**, 60, 345.
- [39] Z. Jiang, W. Sun, H. Shang, W. Chen, T. Sun, H. Li, J. Dong, J. Zhou, Z. Li, Y. Wang, R. Cao, R. Sarangi, Z. Yang, D. Wang, J. Zhang, Y. Li, *Energy Environ. Sci.* **2019**, 12, 3508.
- [40] X. Zhang, Y. Wang, M. Gu, M. Wang, Z. Zhang, W. Pan, Z. Jiang, H. Zheng, M. Lucero, H. Wang, G. E. Sterbinsky, Q. Ma, Y.-G. Wang, Z. Feng, J. Li, H. Dai, Y. Liang, *Nat. Energy* **2020**, 5, 684.
- [41] W. Peng, M. Luo, X. Xu, K. Jiang, M. Peng, D. Chen, T. S. Chan, Y. Tan, *Adv. Energy Mater.* **2020**, 10, 2001364.
- [42] H. Zhong, M. Ghorbani-Asl, K. H. Ly, J. Zhang, J. Ge, M. Wang, Z. Liao, D. Makarov, E. Zschech, E. Brunner, I. M. Weidinger, J. Zhang, A. V. Krashennnikov, S. Kaskel, R. Dong, X. Feng, *Nat. Commun.* **2020**, 11, 1409.
- [43] H. B. Yang, S.-F. Hung, S. Liu, K. Yuan, S. Miao, L. Zhang, X. Huang, H.-Y. Wang, W. Cai, R. Chen, J. Gao, X. Yang, W. Chen, Y. Huang, H. M. Chen, C. M. Li, T. Zhang, B. Liu, *Nat. Energy* **2018**, 3, 140.
- [44] J. Feng, H. Gao, L. Zheng, Z. Chen, S. Zeng, C. Jiang, H. Dong, L. Liu, S. Zhang, X. Zhang, *Nat. Commun.* **2020**, 11, 4341.
- [45] Z. Jiang, T. Wang, J. Pei, H. Shang, D. Zhou, H. Li, J. Dong, Y. Wang, R. Cao, Z. Zhuang, W. Chen, D. Wang, J. Zhang, Y. Li, *Energy Environ. Sci.* **2020**, 13, 2856.
- [46] H. Shang, T. Wang, J. Pei, Z. Jiang, D. Zhou, Y. Wang, H. Li, J. Dong, Z. Zhuang, W. Chen, D. Wang, J. Zhang, Y. Li, *Angew. Chem., Int. Ed.* **2020**, 59, 22465.
- [47] H. Shang, X. Zhou, J. Dong, A. Li, X. Zhao, Q. Liu, Y. Lin, J. Pei, Z. Li, Z. Jiang, D. Zhou, L. Zheng, Y. Wang, J. Zhou, Z. Yang, R. Cao, R. Sarangi, T. Sun, X. Yang, X. Zheng, W. Yan, Z. Zhuang, J. Li, W. Chen, D. Wang, J. Zhang, Y. Li, *Nat. Commun.* **2020**, 11, 3049.
- [48] M. T. Greiner, T. E. Jones, S. Beeg, L. Zwiener, M. Scherzer, F. Girsdiess, S. Piccinin, M. Armbruster, A. Knop-Gericke, R. Schlögl, *Nat. Chem.* **2018**, 10, 1008.
- [49] J. Gu, C.-S. Hsu, L. Bai, H. Chen, X. Hu, *Science* **2019**, 364, 1091.
- [50] J. Jiao, R. Lin, S. Liu, W. C. Cheong, C. Zhang, Z. Chen, Y. Pan, J. Tang, K. Wu, S. F. Hung, H. M. Chen, L. Zheng, Q. Lu, X. Yang, B. Xu, H. Xiao, J. Li, D. Wang, Q. Peng, C. Chen, Y. Li, *Nat. Chem.* **2019**, 11, 222.
- [51] Y. Huang, S. Liu, H. B. Yang, S. F. Hung, J. Ding, W. Z. Cai, L. H. Liu, J. J. Gao, X. N. Li, T. Zhang, B. Liu, X. Y. Ren, Z. C. Kuang, *Angew. Chem., Int. Ed.* **2019**, 59, 798.
- [52] X. Han, T. Zhang, W. Chen, B. Dong, G. Meng, L. Zheng, C. Yang, X. Sun, Z. Zhuang, D. Wang, A. Han, J. Liu, *Adv. Energy Mater.* **2020**, 2002753, <https://doi.org/10.1002/aenm.202002753>.
- [53] M. Wang, S. Liu, T. Qian, J. Liu, J. Zhou, H. Ji, J. Xiong, J. Zhong, C. Yan, *Nat. Commun.* **2019**, 10, 341.
- [54] Z. Li, Y. Chen, S. Ji, Y. Tang, W. Chen, A. Li, J. Zhao, Y. Xiong, Y. Wu, Y. Gong, T. Yao, W. Liu, L. Zheng, J. Dong, Y. Wang, Z. Zhuang, W. Xing, C. T. He, C. Peng, W. C. Cheong, Q. Li, M. Zhang, Z. Chen, N. Fu, X. Gao, W. Zhu, J. Wan, J. Zhang, L. Gu, S. Wei, P. Hu, J. Luo, J. Li, C. Chen, Q. Peng, X. Duan, Y. Huang, X.-M. Chen, D. Wang, Y. Li, *Nat. Chem.* **2020**, 12, 764.
- [55] G. Malta, S. A. Kondrat, S. J. Freakley, C. J. Davies, L. Lu, S. Dawson, A. Thetford, E. K. Gibson, D. J. Morgan, W. Jones, P. P. Wells, P. Johnston, C. R. A. Catlow, C. J. Kiely, G. J. Hutchings, *Science* **2017**, 355, 1399.
- [56] Q. Jia, N. Ramaswamy, H. Hafiz, U. Tylus, K. Strickland, G. Wu, B. Barbiellini, A. Bansil, E. F. Holby, P. Zelenay, S. Mukerjee, *ACS Nano* **2015**, 9, 12496.
- [57] M. Xiao, J. Zhu, L. Ma, Z. Jin, J. Ge, X. Deng, Y. Hou, Q. He, J. Li, Q. Jia, S. Mukerjee, R. Yang, Z. Jiang, D. Su, C. Liu, W. Xing, *ACS Catal.* **2018**, 8, 2824.
- [58] A. Zitolo, N. Ranjbar-Sahraie, T. Mineva, J. Li, Q. Jia, S. Stamatina, G. F. Harrington, S. M. Lyth, P. Krtić, S. Mukerjee, E. Fonda, F. Jaouen, *Nat. Commun.* **2017**, 8, 957.
- [59] K. Jiang, S. Siahrostami, T. Zheng, Y. Hu, S. Hwang, E. Stavitski, Y. Peng, J. Dynes, M. Gangisetty, D. Su, K. Attenkofer, H. Wang, *Energy Environ. Sci.* **2018**, 11, 893.
- [60] T. Sun, S. Zhao, W. Chen, D. Zhai, J. Dong, Y. Wang, S. Zhang, A. Han, L. Gu, R. Yu, X. Wen, H. Ren, L. Xu, C. Chen, Q. Peng, D. Wang, Y. Li, *Proc. Natl Acad. Sci. USA* **2018**, 115, 12692.
- [61] Y. Yao, S. Hu, W. Chen, Z.-Q. Huang, W. Wei, T. Yao, R. Liu, K. Zang, X. Wang, G. Wu, W. Yuan, T. Yuan, B. Zhu, W. Liu, Z. Li, D. He, Z. Xue, Y. Wang, X. Zheng, J. Dong, C.-R. Chang, Y. Chen, X. Hong, J. Luo, S. Wei, W.-X. Li, P. Strasser, Y. Wu, Y. Li, *Nat. Catal.* **2019**, 2, 304.
- [62] J. Huang, N. Hormann, E. Oveisi, A. Loidice, G. L. De Gregorio, O. Andreussi, N. Marzari, R. Buonsanti, *Nat. Commun.* **2018**, 9, 3117.
- [63] Y. Li, F. Cui, M. B. Ross, D. Kim, Y. Sun, P. Yang, *Nano Lett.* **2017**, 17, 1312.
- [64] Y. Zhao, X. Tan, W. Yang, C. Jia, X. Chen, W. Ren, S. C. Smith, C. Zhao, *Angew. Chem., Int. Ed.* **2020**, 59, 21493.
- [65] D. Kim, C. S. Kley, Y. Li, P. Yang, *Proc. Natl Acad. Sci. USA* **2017**, 114, 10560.
- [66] D. Gao, H. Zhou, F. Cai, D. Wang, Y. Hu, B. Jiang, W.-B. Cai, X. Chen, R. Si, F. Yang, S. Miao, J. Wang, G. Wang, X. Bao, *Nano Res.* **2017**, 10, 2181.
- [67] F. Maurer, J. Jelic, J. Wang, A. Gänzler, P. Dolcet, C. Wöll, Y. Wang, F. Stedt, M. Casapu, J.-D. Grunwaldt, *Nat. Catal.* **2020**, 3, 824.

- [68] E. J. Peterson, A. T. DeLaRiva, S. Lin, R. S. Johnson, H. Guo, J. T. Miller, J. Hun Kwak, C. H. Peden, B. Kiefer, L. F. Allard, F. H. Ribeiro, A. K. Datye, *Nat. Commun.* **2014**, 5, 4885.
- [69] B. Yang, C. Liu, A. Halder, E. C. Tyo, A. B. F. Martinson, S. Seifert, P. Zapol, L. A. Curtiss, S. Vajda, *J. Phys. Chem. C* **2017**, 121, 10406.
- [70] H. Wei, X. Liu, A. Wang, L. Zhang, B. Qiao, X. Yang, Y. Huang, S. Miao, J. Liu, T. Zhang, *Nat. Commun.* **2014**, 5, 5634.
- [71] S. Lee, S. Lee, M. D. Kumbhalkar, K. M. Wiaderek, J. Dumesic, R. E. Winans, *ChemCatChem* **2017**, 9, 99.
- [72] S. Lee, S. Lee, D. Gerceker, M. D. Kumbhalkar, K. M. Wiaderek, M. R. Ball, M. Mavrikakis, J. A. Dumesic, R. E. Winans, *Phys. Chem. Chem. Phys.* **2019**, 21, 11740.
- [73] Y. Dai, T. J. Gorey, S. L. Anderson, S. Lee, S. Lee, S. Seifert, R. E. Winans, *J. Phys. Chem. C* **2017**, 121, 361.
- [74] J. Timoshenko, A. Halder, B. Yang, S. Seifert, M. J. Pellin, S. Vajda, A. I. Frenkel, *J. Phys. Chem. C* **2018**, 122, 21686.
- [75] X. Zheng, B. Zhang, P. De Luna, Y. Liang, R. Comin, O. Voznyy, L. Han, F. P. Garcia de Arquer, M. Liu, C. T. Dinh, T. Regier, J. J. Dynes, S. He, H. L. Xin, H. Peng, D. Prendergast, X. Du, E. H. Sargent, *Nat. Chem.* **2018**, 10, 149.
- [76] N. Zhang, X. Feng, D. Rao, X. Deng, L. Cai, B. Qiu, R. Long, Y. Xiong, Y. Lu, Y. Chai, *Nat. Commun.* **2020**, 11, 4066.
- [77] S. Lee, A. Halder, G. A. Ferguson, S. Seifert, R. E. Winans, D. Teschner, R. Schlogl, V. Papaefthimiou, J. Greeley, L. A. Curtiss, S. Vajda, *Nat. Commun.* **2019**, 10, 954.
- [78] S. C. Lin, C. C. Chang, S. Y. Chiu, H. T. Pai, T. Y. Liao, C. S. Hsu, W. H. Chiang, M. K. Tsai, H. M. Chen, *Nat. Commun.* **2020**, 11, 3525.
- [79] H. Xiao, W. A. Goddard, T. Cheng, Y. Liu, *Proc. Natl Acad. Sci. USA* **2017**, 114, E7045.
- [80] R. M. Arán-Ais, F. Scholten, S. Kunze, R. Rizo, B. Roldan Cuenya, *Nat. Energy* **2020**, 5, 317.
- [81] Y. Han, Y. Wang, R. Xu, W. Chen, L. Zheng, A. Han, Y. Zhu, J. Zhang, H. Zhang, J. Luo, C. Chen, Q. Peng, D. Wang, Y. Li, *Energy Environ. Sci.* **2018**, 11, 2348.
- [82] Z. Zhu, H. Yin, Y. Wang, C. H. Chuang, L. Xing, M. Dong, Y. R. Lu, G. Casillas-Garcia, Y. Zheng, S. Chen, Y. Dou, P. Liu, Q. Cheng, H. Zhao, *Adv. Mater.* **2020**, 32, 2004670.
- [83] Z. Lu, B. Wang, Y. Hu, W. Liu, Y. Zhao, R. Yang, Z. Li, J. Luo, B. Chi, Z. Jiang, M. Li, S. Mu, S. Liao, J. Zhang, X. Sun, *Angew. Chem., Int. Ed.* **2019**, 58, 2622.
- [84] L. Jiao, J. Wu, H. Zhong, Y. Zhang, W. Xu, Y. Wu, Y. Chen, H. Yan, Q. Zhang, W. Gu, L. Gu, S. P. Beckman, L. Huang, C. Zhu, *ACS Catal.* **2020**, 10, 6422.
- [85] J. Wu, L. Xiong, B. Zhao, M. Liu, L. Huang, *Small Methods* **2019**, 4, 1900540.
- [86] J. Wu, H. Zhou, Q. Li, M. Chen, J. Wan, N. Zhang, L. Xiong, S. Li, B. Y. Xia, G. Feng, M. Liu, L. Huang, *Adv. Energy Mater.* **2019**, 9, 1900149.
- [87] Y. Xiong, W. Sun, P. Xin, W. Chen, X. Zheng, W. Yan, L. Zheng, J. Dong, J. Zhang, D. Wang, Y. Li, *Adv. Mater.* **2020**, 32, 2000896.
- [88] J. Liu, *ACS Catal.* **2017**, 7, 34.
- [89] K. Qi, M. Chhowalla, D. Voiry, *Mater. Today* **2020**, 40, 173.
- [90] B. Lu, Q. Liu, S. Chen, *ACS Catal.* **2020**, 10, 7584.
- [91] D. Liu, Q. He, S. Ding, L. Song, *Adv. Energy Mater.* **2020**, 10, 2001482.
- [92] G. Wan, X.-M. Lin, J. Wen, W. Zhao, L. Pan, J. Tian, T. Li, H. Chen, J. Shi, *Chem. Mater.* **2018**, 30, 7494.
- [93] S. K. Beaumont, *Phys. Chem. Chem. Phys.* **2020**, 22, 18747.
- [94] H. T. Lien, S. T. Chang, P. T. Chen, D. P. Wong, Y. C. Chang, Y. R. Lu, C. L. Dong, C. H. Wang, K. H. Chen, L. C. Chen, *Nat. Commun.* **2020**, 11, 4233.
- [95] Y. Zhang, B. Ingham, S. Cheong, N. Ariotti, R. D. Tilley, R. Naffa, G. Holmes, D. J. Clarke, S. Prabakar, *Ind. Eng. Chem. Res.* **2018**, 57, 63.



Lingzhe Fang is currently a Ph.D. student under the supervision of Prof. Tao Li in the Department of Chemistry and Biochemistry at Northern Illinois University. He obtained his M.S. degree in 2016 in material science from Nanjing University of Science and Technology in China. His research focuses on cathode materials for Li-S batteries and single-atom catalysts for energy conversion areas.



Soenke Seifert, physicist, is a beamline scientist at Sector 12ID at the Advanced Photon Source at Argonne National Laboratory. He developed and built the SAXS instruments. He is supporting users to perform SAXS/WAXS experiments. Dr. Seifert received his Ph.D. in Polymer Science at the University Hamburg.



Randall E. Winans is a senior scientist in the X-ray Science Division at Argonne National Laboratory. He has developed in situ X-ray techniques to understand the fundamental chemistry of complex disordered solid and solution systems, such as energy storage materials, catalysts, soot, heavy petroleum, oil shale and carbons. Chemistry is combined with characterization techniques, including mass spectrometry, IR and X-ray scattering, and spectroscopy. IR and MS are used simultaneously with X-ray techniques. In 2009, he was elected to the inaugural class of the ACS Fellows and was the chair of the 2018 International Conference on Small-Angle Scattering.



Tao Li is an assistant professor in the Department of Chemistry and Biochemistry at Northern Illinois University and holds a joint assistant scientist position at the Advanced Photon Source at Argonne National Lab. His research interests focus on using advanced X-ray techniques to study nanoparticles and energy materials' self-assembly, including catalysts and batteries. Prof. Li completed his Ph.D. in the Department of Chemistry and Biochemistry at the University of South Carolina-Columbia in 2009.